30th NENE 2021
September 6 - 9
BLED-SLOVENIA
International Conference Nuclear Energy for New Europe

CFD analysis of actively cooled divertor target element for stellarator W7-X

Luka Selan, Boštjan Končar
Reactor Engineering Division, Jožef Stefan Institute
Ljubljana, Slovenija
luka.selan97@gmail.com, bostjan.koncar@ijs.si

Jörg Tretter, Jean Boscary
Max-Planck-Institut für Plasmaphysik
Garching, Germany
joerg.tretter@ipp.mpg.de, jean.boscary@ipp.mpg.de

Marianne Richou
CEA, IRFM, CEA-Cadarache
13108 Saint-Paul-lez-Durance, France
marianne.richou@cea.fr

ABSTRACT

The study focuses on the CFD analysis of a possible prototype of water-cooled divertor element for the experimental stellarator-type fusion machine Wendelstein W7-X. The coupled solid-fluid analysis was performed on the selected type of divertor target element. The single-fluid modelling approach was used to explore the effect of the cooling water on the local wall temperature distribution in the cooling channel. Comparison of the wall temperature profile with the local coolant saturation temperature at critical location is presented to detect local superheating regions that may lead to the evolution of boiling flow. The effect of two different heat flux profiles, material of the tiles (tungsten or tungsten heavy alloy) and the effect of the twisted tape was investigated. Maximum temperatures of target materials were compared. The results also included analysis of cooling channel parameters (e.g. superheating, water temperature distribution, pressure drop) and temperature distribution in the cooling channel wall. It is interesting to note that the maximum velocity region is not necessarily located just below the heated wall, but rather near the bottom of the pipe in the colder flow region. The single-fluid results show the necessity to perform realistic simulations in the two-phase flow regime.

1 INTRODUCTION

Wendelstein W7-X (W7-X) is the largest and most advanced stellarator-type experimental fusion machine located in Greifswald, Germany. W7-X started first divertor operation with short-pulses with an adiabatically loaded divertor armored with fine graphite tiles. The next step is long-pulse operation with pulse length up to 1800 sec. and continuous plasma heating with up to 10 MW electron cyclotron resonance heating (ECRH). To operate in these conditions, an actively water-cooled high heat flux divertor needs to be installed.

The divertor is made of the target elements. The design of a target element is based on the flat tile technology. A CuCrZr copper alloy heat sink is armoured with carbon fibre reinforced carbon (CFC) tiles and was designed to remove a stationary heat flux of 10 MW/m². The design and manufacturing route of the target elements was qualified by an extensive pre-qualification programme [1]. However, CFC is not a plasma facing material relevant to a reactor and the next generation of divertor target elements of W7-X is planned to be armoured with tungsten or tungsten alloy. The design of the water-cooled CFC divertor presently installed in W7-X is shown in Figure 1.

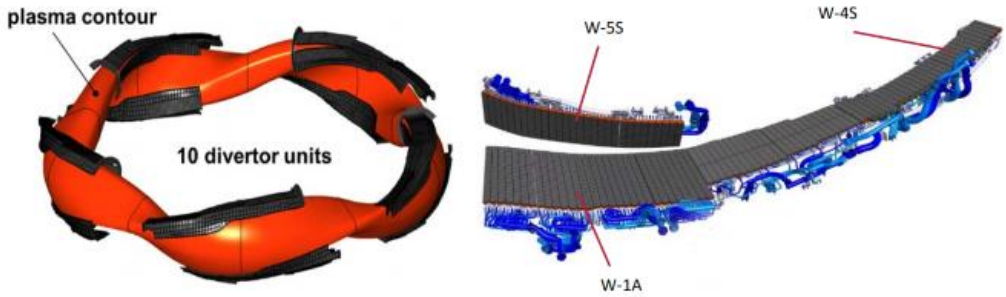

Figure 1: Position of divertor units along the helicoidal plasma of W7-X (left) [2] ; Close-up view of one CFC divertor unit (right) [3]

The first preliminary approach to design the next generation of target elements for W7-X is the replacement of the CFC tiles by tungsten / tungsten alloy tiles, while keeping the same heat sink. The type of target element W-4S has been selected to carry out the first calculations in order to support the design and specification of the first prototypes.

In this study CFD simulations of the divertor target geometries W-4S-011 (without twisted tape) and W-4S-111 (with twisted tape) were performed. The single-fluid modelling approach was used to simulate the cooling water flow and its effect on wall temperature distribution of the cooling channel. Comparison of the wall temperature profile with the local coolant saturation temperature at critical location is presented to detect local superheating regions that may lead to the evolution of boiling flow. The influence of two different stationary heat loads, tile material and twisted tape insertion on the overall temperature distribution is analysed.

2 DESIGN AND MATERIALS OF THE TARGET ELEMENT

The preliminary possible design of the W-4S prototype consists of a CuCrZr heat sink of slightly trapezoidal shape with main dimensions 260x56x19 mm and with a 9 mm cooling channel. On the plasma facing side, above the heat sink, there is a 2 mm thick Cu interlayer with 3.5 mm thick W or W alloy tiles on top of it. The twisted tape inside the cooling channel has a thickness of 1 mm and a twist ratio of 2. The geometry model of the prototype, prepared at Max-Planck-Institut für Plasmaphysik [4], is shown in Figure 2.

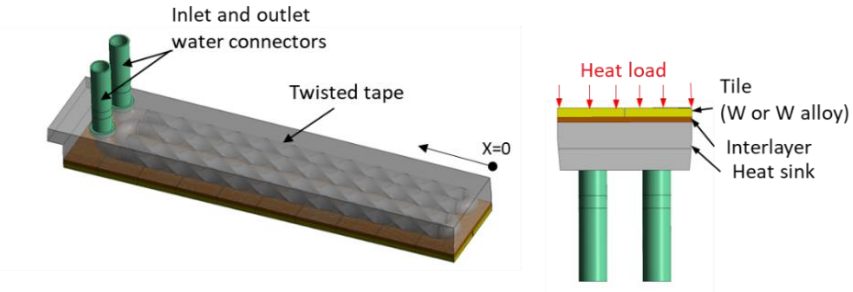

Figure 2: Geometry model of the W-4S-111 target element [4] (left), front view (right)

The specific heat capacity, density and thermal conductivity of target materials are considered as temperature dependent [5]. For water, all the properties are taken from IAPWS tables [6] integrated in ANSYS CFX solver [7].

3 NUMERICAL MODEL

3.1 Mathematical model

A conjugate heat transfer model for the fluid and solid need to be solved. The mathematical model for the fluid consists of conservation equations for mass, momentum and energy that are based on Reynolds averaging of the Navier-Stokes equations. It should be noted that in this study, the fluid is considered only as a single-phase turbulent flow (the Reynolds number is around 100000). The turbulence in the fluid domain is modelled by the two-equation eddy viscosity k-ω Shear Stress Transport (SST) model. The model incorporates k-ω model in the near-wall regions and the standard k-ε model in the fully turbulent region. The model is further improved with model constants, blending functions and eddy viscosity limiters [8]. The transport of turbulence kinetic energy and specific dissipation rate is described by Eq. (1) and Eq. (2), respectively, according to [9].

$$\frac{\partial k}{\partial t} + U_j \frac{\partial k}{\partial x_j} = P_k - \beta^* k\omega + \frac{\partial}{\partial x_j}\left[(\nu + \sigma_k \nu_T)\frac{\partial k}{\partial x_j}\right], \quad (1)$$

$$\frac{\partial \omega}{\partial t} + U_j \frac{\partial \omega}{\partial x_j} = \alpha S^2 - \beta\omega^2 + \frac{\partial}{\partial x_j}\left[(\nu + \sigma_\omega \nu_T)\frac{\partial \omega}{\partial x_j}\right] + 2(1 - F_1)\sigma_{\omega 2}\frac{1}{\omega}\frac{\partial k}{\partial x_i}\frac{\partial \omega}{\partial x_i}, \quad (2)$$

where α, β^*, β, σ_k, σ_ω and $\sigma_{\omega 2}$ are model parameters, P_k is the production term of the turbulent kinetic energy k, S is the magnitude of the first velocity derivative and ω is the turbulence eddy frequency. The function F_1 is the first blending function in the SST model that is 1 inside the boundary layer and 0 in the core flow. Variable U_j presents the mean velocity component. The k-ω SST turbulence model has been widely used and validated for simulation of pipe flows and swirling boundary layer flows [10],[11],[12], similar to the flow conditions in this study.

3.2 Model settings and heat loading

ANSYS CFX solver was used to perform the simulations [7]. The solver is set to high resolution scheme for advection terms and to first order numerics for the turbulence equations. The convergence criteria are set to maximum residual type with 10^{-5} residual target to minimize the numerical mass and energy imbalance.

The water flows into the connector at 30˚C and at a fixed mass flow rate of 0.57 kg/s reaching the average velocity of 9 m/s inside the cooling channel. At the outlet the pressure is set to 1 MPa. Two different heat loads are applied to the plasma facing surface, one denoted as "HHF", with a constant heat flux of 10 MW/m^2 on the limited region of the target surface and the other, denoted as "High-Iota_1", with an approximated heat flux profile across the whole target surface with a maximum peak of 10 MW/m^2 based on the analysis of first operation of W7-X. The heat loads along the x-axis are shown in Figure 3 (the x=0 point is marked on Figure 2). The heat flux is constant in the transverse direction.

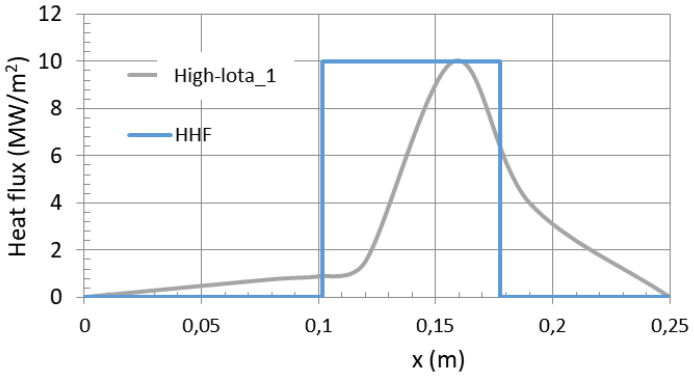

Figure 3: Heat load of the plasma facing components

3.3 Mesh

The first step before the mesh generation required simplifying the geometry model, using the steps like removing the chamfers, thread connections and other features not vital in the heat transfer analysis. This simplified the mesh generation and simulations without affecting the simulation results. Mesh was generated with ANSYS mesh software [7]. As shown in Figure 4, hexagonal meshing is applied for tiles, while the tetra mesh is used for the remaining solid domains due to the more complex geometry. The mesh is refined in the interlayer, at the upper part of the heat sink and at the interfaces to be able to capture the high temperature gradients. In the fluid domain, the mesh is refined at the fluid-solid interfaces using the inflated prism layers to ensure sufficiently accurate solution of the velocity and temperature gradients in the near-wall region of the fluid domain. The mesh cross-section of the divertor target element with the twisted tape is presented in Figure 4 (left). The mesh of the target element with the twisted tape consists of 17,735,966 mesh cells and the mesh without it consists of 13,166,598 cells. These meshes are based on the preliminary mesh refinement analysis.

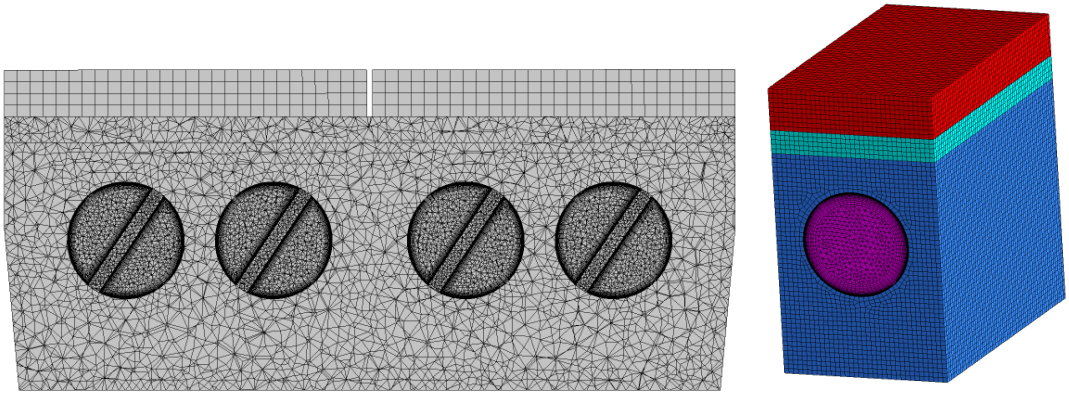

Figure 4: The mesh cross-section of the target element with the twisted tape (left) and the fine mesh of the small model used for mesh sensitivity analysis (right)

To avoid excessively long computational times, the mesh sensitivity analysis was performed on the representative “small model”, which includes one cut-out of the target element with a single pipe section without the twisted tape. Three different meshes were created, coarse, medium and fine with different element sizes and fluid inflation layers. The density of the medium mesh is approximately similar to the one used in the simulations of the whole target element. The resulting temperatures and mesh parameters are shown in Table 1. The mesh analysis shows that decreased size of the first near-wall layer increases the maximum fluid temperature, which approaches to the wall temperature. Decreasing the element size by a factor

of 4 reduced maximum temperatures of solid components when comparing coarse and medium meshes. Further refinement (going from medium to the fine mesh) however tends to slightly increase the material temperatures. The results on the medium mesh show a good compromise between the desired accuracy and still manageable computational time. The discrepancy between the fine and the medium mesh amounts 5°C for the maximum tile temperature and 10°C for the maximum wall temperature.

Table 1: Mesh sensitivity analysis on the "small model"

Case name	Coarse mesh	Medium mesh	Fine mesh
Mesh elements	18,828	352,961	13,470,267
Element size[mm]	1.6	0.4	0.1
First inflation layer[mm]	0.08	0.008	0.0008
$T_{wall\_max} - T_{sat}$ [°C]*	66	33	43
T_{out} Fluid [°C]	82	129	215
T_{max} Tube wall [°C]	247	214	224
T_{max} Tile [°C]	660	625	630
T_{max} Interlayer [°C]	388	358	361
T_{max} Heat Sink [°C]	336	306	309

*Difference between the maximum pipe wall temperature and local fluid saturation temperature

4 RESULTS AND DISCUSSION

Four different cases have been analysed, with the coolant flow treated as a single-phase fluid. The two cases with tungsten tiles (W HHF and W P1) have no twisted tape and are simulated with two different heat flux profiles (see Figure 3). The other two cases with tiles made of tungsten alloy (W35Ni15Cu) have been simulated either with or without the twisted tape (WCN HHF or WCN HHF). For both cases a constant heat load (HHF) is applied. The main simulation results are presented in Table 2. The predicted maximum temperatures of the solid materials are below the melting points of corresponding structure materials in all simulated cases (W/W35Ni15Cu- 3410°C, Cu/CuCrZr- 1.085 °C).

Table 2: Simulation results

Case Name	W HHF	W P1	WCN HHF	WCN-S HHF
Tile material	W	W	W35Cu15Ni	W35Cu15Ni
Heat flux load	HHF	High-Iota_1	HHF	HHF
Twisted tape	No	No	No	Yes
dp[bar]	2.5	2.4	2.4	6.2
$T_{wall\_max} - T_{sat}$ [°C]*	57	46	64	10
T_{max} Fluid [°C]	98	78	97	87
T_{max} Tube wall [°C]	239	227	247	192
T_{max} Tile [°C]	668	626	811	762
T_{max} Interlayer [°C]	397	368	406	358
T_{max} Heat Sink [°C]	346	319	355	308

*Difference between the maximum pipe wall temperature and local fluid saturation temperature defines maximum wall superheating
*W/WCN-Tungsten/Tungsten alloy material, HHF/P1- High heat flux/Iota 1-heat flux load, S-swirl tape

The effect of heat flux profile for the W tile design is shown in the first two columns of Table 2. The maximum tile temperature is 42˚C lower in the case of the operation High-Iota_1

profile (W P1). The maximum temperatures of other materials (interlayer and heat sink) are also reduced.

The difference between the two cases with different tile materials for the same loading conditions can be seen by comparing the first and the third column of the Table 2 (W HHF and WCN HHF). The maximum temperature of the tungsten tile (W HHF) lower by 143˚C due to the higher thermal conductivity of the tungsten compared to the tungsten alloy. The maximum temperatures of the interlayer, heat sink and the maximum temperature of the cooling channel wall are changed by less than 10˚C, since the conditions in the coolant remain approximately the same.

The effect of twisted tape on the maximum temperatures is analysed for the W alloy case (WCN HHF and WCN-S HHF) in the last two columns of Table 2. The insertion of the twisted tapes increases the heat transfer between the pipe wall and the water coolant and significantly reduces the maximum wall temperatures, from 247 ˚C to 192˚C. Consequently, the peak temperatures of the tile, interlayer and heat sink are reduced by 49˚C, 52˚C and 47˚C, respectively. On the other hand, the twisted tapes increase the pressure drop in the cooling channels from 2.4 bar to 6.2 bar. The wall temperature distributions on the channel surface and the velocity distributions at the fluid cross-section (located at the tile temperature peak) are shown in Figure 5. It is interesting to note that the maximum velocity region is not necessarily located just below the heated wall, but rather near the bottom of the pipe in the colder flow region. This may be attributed to the stronger local mixing in the hot fluid region, which hinders the dominant streamwise velocity component.

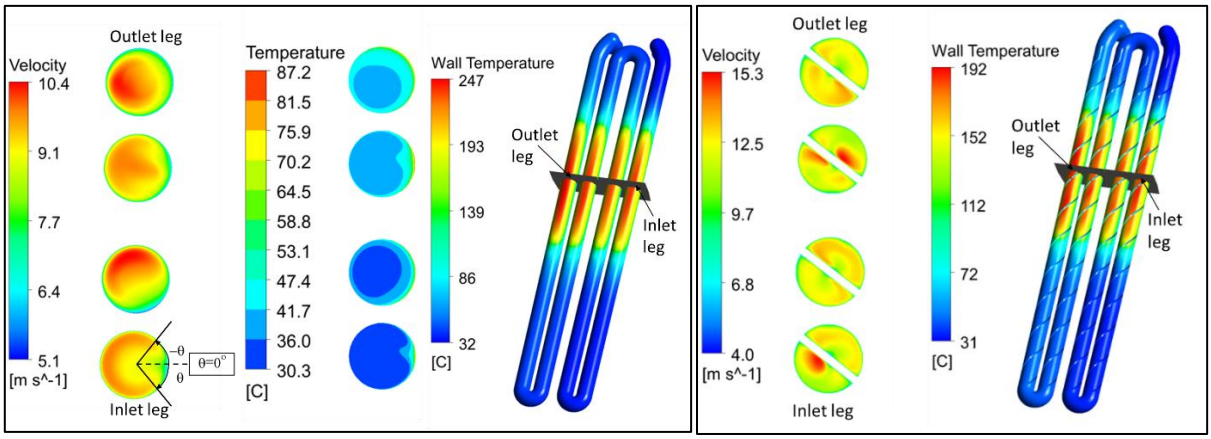

Figure 5: W35Ni1Cu tile, HHF case: Velocity and fluid temperature distribution at the fluid cross-section, temperature distribution on the pipe wall (case without twisted tape - left); velocity at the fluid cross-section and pipe wall temperature (case with twisted tape - right)

The possibility of local boiling occurrence is investigated in Figures 6 and 7, where the circumferential distribution of the pipe wall temperature at the critical cross-section (maximum tile temperature) is compared against the local saturation temperature. The wall temperature distributions on the pipe cross-section are shown for the inlet and outlet leg of the cooling channel. The cross-sectional plane is shown in Figure 5. The effect of heat flux profile for the W tile is presented in Figure 6. The circumferential wall temperature profile is asymmetric. The temperatures are always higher on the adiabatic side than on the side close to the adjacent cooling channel. At the outlet leg, the wall temperature exceeds the local saturation temperature in the range from -60^o to 40^o (0^o is exactly below the top of the channel). The highest superheating exceeds 50^{o}C and is slightly shifted from the center of the channel. The two-phase flow is very likely to occur in this superheated region. The range of superheating and its

maximum value is slightly lower in the case of W P1, and less severe for both cases at the inlet leg.

The effect of the twisted tape for the W alloy tile design is presented in Figure 7. In the case without the twisted tape the superheating region at the outlet leg is even wider (from about -75° to 50°) with a higher maximum superheating (over 60 °C). Insertion of the twisted tape (WCN-S HHF case) significantly reduces the superheating range (-30° to 15°) as well as the maximum superheating value (~ 10 °C). Superheating region completely disappears at the inlet leg.

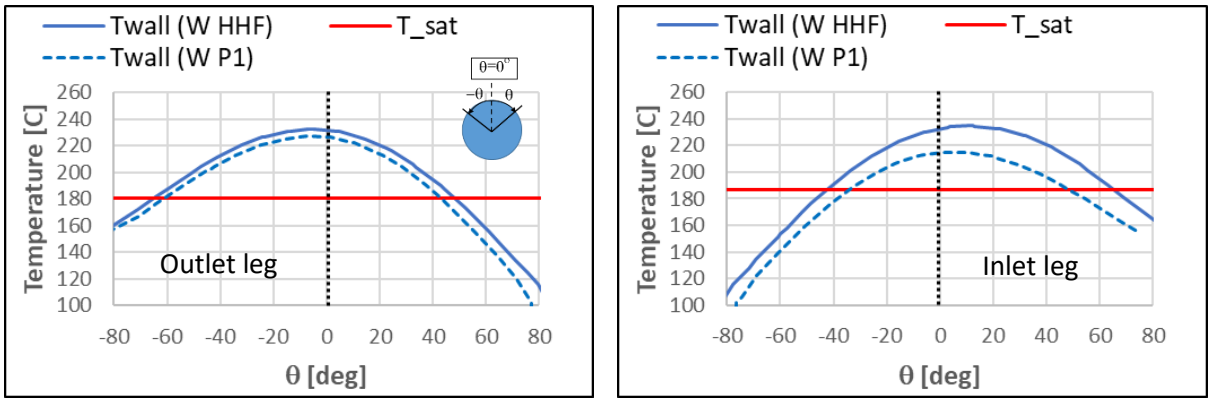

Figure 6: Effect of heat flux profile (W tile): Wall temperature distribution along the circumference of the pipe is compared with the saturation temperature (red line). Blue dotted line presents the "High-Iota_1" heat flux profile. Outlet leg (left) and inlet leg (right) cross-sections are shown.

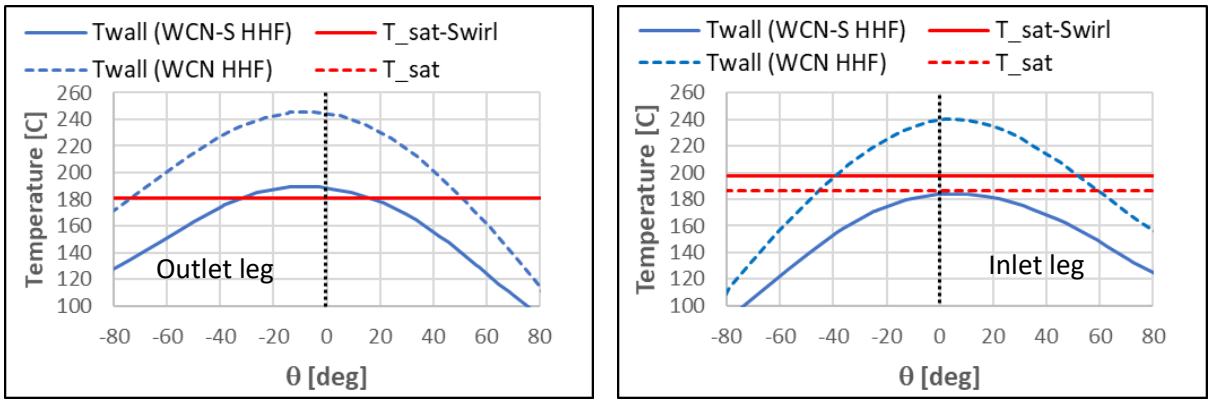

Figure 7: Effect of twisted tape (W35Cu15Ni tile, HHF case): Wall temperature distributions (blue lines) along the circumference of the pipe are compared with the saturation temperature (red lines). Full and dotted lines present the results with and without the twisted tape, respectively. Outlet leg (left) and inlet leg (right) cross-sections are shown.

5 CONCLUSIONS

The CFD analysis of the selected W7-X divertor target element has been performed using the single-phase fluid approach to model the water coolant. The influence of heat flux profile, material off the tiles (tungsten or tungsten alloy) and the effect of twisted tape was investigated. In general, the results indicate that the temperatures of the target element materials are always below the critical values. The main focus was given on studying the local superheating regions on the cooling channel wall that may lead to local boiling conditions. The main results can be summarized as follows:

- The twisted tapes in the cooling channel significantly reduced the maximum temperatures of all target materials, but also significantly increased the pressure drop in the cooling channel, from 2.4 to 6.2 bar. The twisted tape decreased the pipe wall temperature (T_{wall}) below the saturation temperature (T_{sat}) at the inlet leg, still some local superheating (by ~10^{o}C) can be observed at the outlet leg.
- The circumferential distribution of T_{wall} is asymmetric with higher values at the adiabatic side of the target element. At the outlet leg the superheating occurs approximately in the range of circumferential angles between -75^{o} and 50^{o} for WCN HHF case and between -30^{o} to 15^{o} for WCN-S HHF case.

The single-fluid results show the necessity to perform realistic simulations in the two-phase flow regime.

ACKNOWLEDGMENTS

The present work has been carried out within the framework of the EUROfusion Consortium and has received funding from the Euratom research and training programme 2014-2018 and 2019-2020 under grant agreement No. 633053. The views and opinions expressed herein do not necessarily reflect those of the European Commission.

The financial support provided by the Slovenian Research Agency, grants J2-9209, P2-0405 and P2-0026 is gratefully acknowledged.

REFERENCES

[1] H. Greuner, B. Böswirth, J. Boscary, T. Friedrich, C. Lavergne, C. Linsmeier, J. Schlosser in A. Wiltner, „Review of the high heat flux testing as an integrated part of W7-X divertor," Fusion Eng. Design, 84, 2009.

[2] T. S. Pedersen, R. König, M. Krychowiak, M. Jakubowski, J. Baldzuhn, S. Bozhenkov, G. Fuchert, A. Langenberg, H. Niemann, D. Zhang, K. Rahbarnia, H.-S. Bosch, Y. Kazakov in S. Brezinsek, „First results from divertor operation in Wendelstein 7-X," Plasma Physics and Controlled Fusion, 61, 2019.

[3] J. Boscary, G. Ehrke, H. Greuner, P. Junghanns, C. Li, B. Mendelevitch, J. Springer in R. Stadler, „Completion of the production of the W7-X divertor target modules," Fusion Eng. Design, 166, 2021.

[4] J. Boscary, Personal correspondence to B. Končar and L. Selan: Updated Input for DIV-W7X.S.3-T001-D002, Avg. 2021.

[5] K. Zhang, Personal correspondence to B. Končar and J. Boscary: Material data, Jul. 2021.

[6] The International Association for the Properties of Water and Steam, Revised Release on the IAPWS Industrial Formulation 1997 for the Thermodynamic Properties of Water and Steam, 2007.

[7] ANSYS documentation, release 2019, User guide, 2019.

[8] H. Versteeg in W. Malalasekera, An Introduction to Computational Fluid Dynamics; Finite volume method, Pearson Education Limited, 2007.

[9] F. R. Menter, „Two.equation eddy-viscosity turbulence models for engineering applications," AIAA Journal, 32, No. 8, 1994.

[10] B. Končar in S. Košmrlj, „Simulation of turbulent flow in MATIS-H rod bundle with split-type mixing vanes," Nuclear Eng. Design, 327, pp. 112-116, 2018.

[11] E. Clark, A. Lumsdaine, J. Boscary, H. Greuner in K. Ekici, „Thermal-hydraulics modeling for prototype testing of the W7-X high heat flux scraper element," Fusion Eng. Design, 121, pp. 211–217, 2017.

[12] P. Zacha in S. Entler, „High heat flux limits of the fusion reactor water-cooled first wall," Nuclear Eng. Technology, 51, pp. 1251-1260, 2019.